Ferroelectric domain structures around the morphotropic phase boundary of the piezoelectric material $PbZr_{1-x}Ti_xO_3$

Toshihiro Asada[1,2] and Yasumasa Koyama[2]
[1]*Research Department, NISSAN ARC, LTD., Yokosuka, Kanagawa 237-0061, Japan*
[2]*Kagami Memorial Laboratory for Materials Science and Technology and Department of Materials Science and Engineering, Waseda University, Tokyo 169-0051, Japan*

(Received 20 July 2005; revised manuscript received 13 May 2007; published 20 June 2007)

In the simple perovskite oxide $PbZr_{1-x}Ti_xO_3$ (PZT), an excellent piezoelectric response was obtained in the vicinity of a morphotropic phase boundary (MPB) between the ferroelectric monoclinic (F_M) and rhombohedral (F_R) phases. In order to understand the origin of this exceptional response, we have used transmission electron microscopy to investigate the detailed features of the ferroelectric domain structures near the MPB in PZT. Two types of domain structures, domains I and II, existed at room temperature in the F_M side of the MPB, while the room-temperature structure in the F_R side was confirmed to be a usual structure consisting of the 109° and 180° domain boundaries. The notable feature of these domain structures is that each domain in both the domain II and the F_R domain structure near the MPB can be identified as an aggregation of nanometer domains with an average size of about 10 nm. In order to clarify the formation of these domain structures, we conducted *in situ* observations from room temperature to about 800 K. The results revealed that the usual F_R domain structure at room temperature was produced by a conversion from a nanometer-sized domain structure consisting of nanometer ferroelectric domains, which formed just below the Curie temperature. The characteristic feature of the nanometer-sized structure is that nanometer regions with the [001] or $[00\bar{1}]$ polarization component were uniformly distributed in a large [110]-component area. Because spatial average of ⟨001⟩ components must be zero in a large [110]-component area, the nanometer-sized domain structure may have an average [110] polarization with average orthorhombic symmetry. In the F_M side, on the other hand, a new banded domain structure appeared in the interior of each domain of domain II on heating at a temperature T_T, but basically disappeared at T_T on subsequent cooling. This reversible change in the banded structure indicates that a phase transition occurs at T_T. Because the banded domain structure appeared in the heating process, the higher- and lower-temperature phases may have triclinic and monoclinic symmetries, respectively. In addition, a similar banded domain structure was observed in a poled sample. On the basis of the existence of this feature, we believe that the presence of the triclinic phase near the MPB may be the crucial factor responsible for the excellent piezoelectric response in PZT.

DOI: 10.1103/PhysRevB.75.214111 PACS number(s): 77.84.Dy, 64.70.Kb, 68.37.Lp

I. INTRODUCTION

Piezoelectric materials acting as converters between mechanical and electrical energies have gained importance through recent applications in fields such as medical imaging.[1–3] The simple perovskite oxide $PbZr_{1-x}Ti_xO_3$ (PZT) is known to exhibit an excellent piezoelectric response near the morphotropic phase boundary (MPB) between the ferroelectric tetragonal (F_T) and rhombohedral (F_R) phases around $x=0.50$.[4]

Many efforts have been undertaken to understand the origin of the excellent response in PZT.[5–8] Recent synchrotron x-ray powder diffraction experiments done by Noheda *et al.* showed the existence of a ferroelectric monoclinic (F_M) phase in the F_R side of the MPB.[9–13] Figure 1 provides their reported phase diagram of PZT in the vicinity of the MPB. According to the diagram, the F_M phase appears via the F_T phase in the cooling process from the paraelectric cubic (P_C) phase, and the F_M/F_R phase boundary is almost independent of temperature. On the basis of the latter finding, the F_M/F_R boundary, rather than the F_T/F_M one, can be identified as the MPB. In addition, Bellaiche *et al.* used an *ab initio* approach to calculate the polarization rotation and the d_{33} piezoelectric coefficient by applying an electric field of [111] orientation to the F_T phase with [001] polarization.[14] They found a sharp peak of the d_{33} coefficient at the F_M/F_R phase boundary, that is, at the MPB. Thus the large piezoelectric response in PZT seems to be directly associated with the polarization rotation in the F_M phase.

The excellent piezoelectric response near the MPB in PZT was obtained in poled samples, to which an external electric field was applied. It is known that the poling treatment usually results in a preferred arrangement of ferroelectric domains in response to an applied electric field. Furthermore, in the case of the F_M phase, the treatment should rotate the direction of a polarization vector in the {110} planes. In fact, as mentioned earlier, the polarization rotation in the F_M phase has been discussed theoretically. However, the detailed features of both the ferroelectric domain structures near the MPB and their changes as a function of temperature remain unknown. Because any direction in the {110} planes is basically allowed as a polarization direction in the F_M phase, local fluctuations of a polarization vector may result in a unique domain structure, such as a structure consisting of nanometer ferroelectric domains. With this motivation, we have used transmission electron microscopy to investigate the crystallographic features of the ferroelectric domain

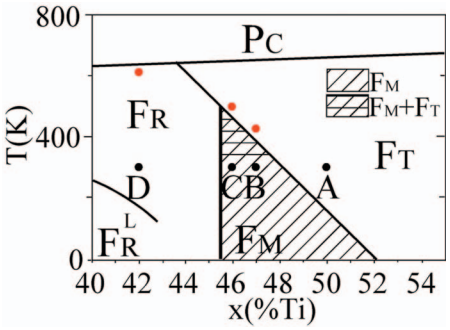

FIG. 1. (Color) Reported phase diagram of PZT near the MPB (Ref. 12). In the diagram, the red circles denote the temperatures, at which the domain-structures changes occurred in the present PZT samples with $x=0.47$ (B), 0.46 (C), and 0.42 (D).

structures near the MPB in PZT and their changes with respect to temperature and external electric field.

II. EXPERIMENTAL PROCEDURE

In this study, $PbZr_{1-x}Ti_xO_3$ (PZT) samples with $0.38 \leqslant x \leqslant 0.52$ were prepared by a conventional solid-state reaction. Initial powders of PbO, ZrO_2, and TiO_2 were first mixed by ball milling for 16 h and pressed into pellets. After calcining at 1173 K for 1 h, the pellets were crushed, mixed for 16 h, and pressed into pellets again. Then they were sintered at 1448 K for 16 h. These sintered samples were provided for dielectric measurements and transmission-electron-microscopy observation.

The characterization of the dielectric properties of the samples obtained in this study was accomplished by the measurement of their real dielectric permittivities. We carried out the measurement with a HIOKI 3532 LCR meter between room temperature and about 730 K for frequencies of 1 kHz–1 MHz. In order to examine the features of the ferroelectric domain structures in these samples, we used a JEM-3010 transmission electron microscope with an accelerating voltage of 300 kV to take their electron diffraction patterns, and bright- and dark-field images between room temperature and about 800 K. Ar-ion milled samples coated with carbon films were provided for our observation. Note that the carbon coating was applied to avoid charging. The average thickness of samples for observation was estimated to be about 100 nm. Imaging plates were also used as a recording medium to prevent specimen drift during observation.

An important feature of this experiment was our determination of the direction of a polarization vector in each ferroelectric domain through the failure of Friedel's law under a two-beam condition.[15,16] The details of the method have been provided in our previous papers.[17] Furthermore, in order to understand the correlation between the excellent piezoelectric response and the domain structure, we examined the characteristic features of a ferroelectric domain structure in poled samples with $x=0.46$. To obtain the poled samples, we first heated them from room temperature to about 450 K, and then cooled them down under an electric field of about 30 kV/cm.

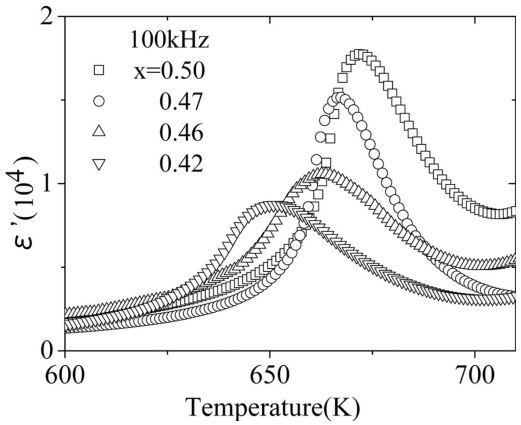

FIG. 2. Temperature dependence of the real dielectric permittivity ε' with 100 kHz in the cooling process for the $x=0.50$, 0.47, 0.46, and 0.42 samples.

III. EXPERIMENTAL RESULTS

A. Dielectric properties

In this study, we first confirmed the dielectric properties of the prepared PZT samples. Before describing the features of the ferroelectric domain structures found in the F_T, F_M, and F_R phases, we here report the temperature dependence of the real dielectric permittivity ε' for the samples with $0.42 \leqslant x \leqslant 0.52$. Measured values of ε' at 100 kHz for the $x=0.50$, 0.47, 0.46, and 0.42 samples in the cooling process are plotted in Fig. 2. Note that the $x=0.50$, 0.47, 0.46, and 0.42 samples, respectively, have the F_T, F_M, F_M, and F_R phases at room temperature. As the figure shows, each sample exhibits a dielectric peak at the Curie temperature T_C, which is identical to that shown in the phase diagram of Fig. 1. The interesting features are that the temperature of the peak maxiumum decreases as the Ti content x falls, and that a relatively lower and broader peak is observed in the $x=0.42$ and 0.46 samples. On the basis of this feature, it is suggested that the behavior of the ferroelectric transition should be unique for the $x=0.42$ and 0.46 samples near the MPB.

B. Ferroelectric domain structures at room temperature

To clarify these dielectric features, we investigated the detailed crystallographic characteristics of the ferroelectric domain structures in the F_T, F_M, and F_R phases by transmission electron microscopy. The dark field images for the $x=0.50$, 0.47, 0.46, and 0.42 samples, indicated by letters A, B, C, and D in Fig. 1, are shown in Fig. 3. We first see the tetragonal domain structure in image (A) of the $x=0.50$ sample, taken at room temperature using the 002 reflection in the [100] electron incidence. Note that, in this paper, both reflections and electron incidences in electron diffraction patterns are indexed in terms of the pseudocubic notation. In addition, to determine the direction of the polarization vector indicated by the arrow in each ferroelectric domain, we used the fact that, in the two-beam condition, a domain with a polarization vector $\mathbf{P}$ gives rise to bright contrast for $\mathbf{g}\cdot\mathbf{P}>0$, where $\mathbf{g}$ is a scattering vector.[15–17] In image (A) of the

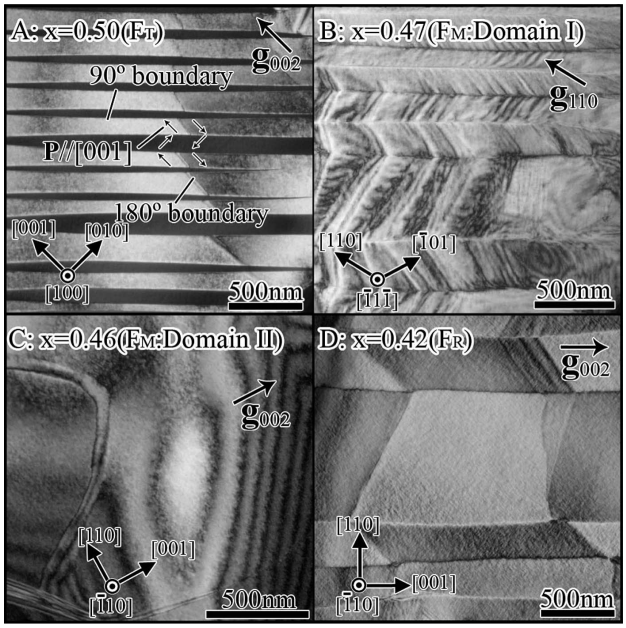

FIG. 3. Four types of ferroelectric domain structures observed at room temperature. Dark field images show the domain structures of the F_T, F_M, and F_R phases in the PZT samples indicated by letters A, B, C, and D in Fig. 1.

F_T phase, as a result of the domain-structure analysis, the usual 90° and 180° domain boundaries are clearly visible in the F_T domain structure.

Two types of domain structures, domains I and II, appear in the the F_M-phase images of the $x=0.47$ and 0.46 samples at room temperature. These images of the $x=0.47$ and 0.46 samples were, respectively, taken by using the 110 reflection in the $[\bar{1}1\bar{1}]$ incidence direction and the 002 reflection in the $[\bar{1}10]$ direction. As is seen in image (B), the domain I observed in $0.47 \leqslant x \leqslant 0.50$ exhibits a herringbone-type morphology consisting of both the banded and striation contrasts. It is worth noticing that the banded contrast is quite similar to that in the 90° domain structure in the F_T phase. In other words, the striation contrast indicated by the arrow seems to be produced by the introduction of one of the ⟨110⟩ components to the [001] polarization in the F_T phase. On the other hand, domain II with curved domain boundaries mainly appears around $x=0.46$ near the MPB, and is not obviously a usual ferroelectric domain structure. The characteristic features of domain II are that many bright-contrast spotty areas with an average size of about 10 nm exist in the interior of each domain, and that the spotty areas tend to align along the [111] direction. On the basis of these features, thus, it seems that each domain in domain II can be identified as an aggregation of nanometer spotty areas.

The F_R domain structure at room temperature near the MPB is seen in image (D), taken from the $x=0.42$ sample, using the 002 reflection in the $[\bar{1}10]$ electron incidence. A usual F_R domain structure with straight domain boundaries is clearly observed in the image. An interesting feature is, however, that many nanometer spotty areas are detected in each F_R domain, just as in the case of domain II in the F_M phase.

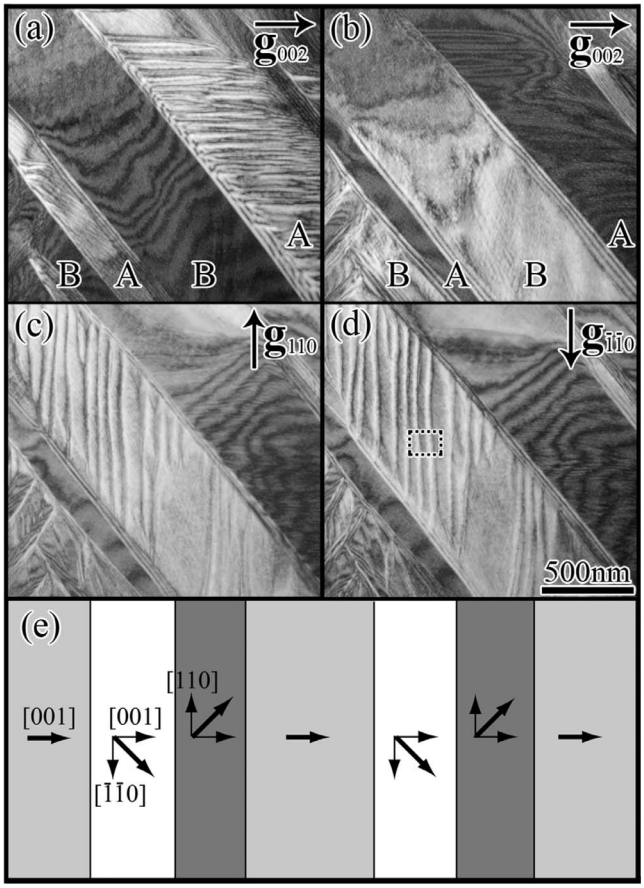

FIG. 4. G-vector dependence of contrast in the dark field images for domain I in the F_M phase, together with a model of domain I. These images were taken from the $x=0.47$ sample at room temperature, using the (a) 002_A, (b) 002_B, (c) 110_B and (d) $1\bar{1}0_B$ reflections, where the subscripts, A and B, indicate two original tetragonal variants. In (e), the resultant polarization-vector directions produced by a sum of [001] and ⟨110⟩ components are denoted by the heavy arrows.

Although the details of the domain-structure analysis for the F_R phase will be described later, these features seem to indicate that the difference between the domain structures in the F_M and F_R phases near the MPB is simply in the straightness of the domain boundary. In other words, if each spotty area corresponds to a nanometer ferroelectric domain, each domain in the F_M and F_R domain structures appearing near the MPB can be identified as an aggregation of nanometer ferroelectric domains. In any case, the characteristic features of the domain structures at room temperature appear to be quite compatible with those of the dielectric properties mentioned before.

C. Crystallographic features of domain I in F_M phase

Of the two monoclinic domain structures at room temperature, we here describe the results of a domain-structure analysis for domain I. The analysis was conducted by taking dark field images with various **g** vectors. Figure 4 shows four dark field images obtained from the same area in the x

=0.47 sample, together with the schematic diagram for the determined domain-structure model. The images in (a)–(d) were, respectively, taken with $\mathbf{g}=002_A$, 002_B, 110_B, and $\bar{1}\bar{1}0_B$ in the $[\bar{1}10]$ electron incidence direction. Note that subscripts A and B denote two original tetragonal variants. In the (a) and (b) images with $\mathbf{g}=002_A$ and 002_B, the banded contrast is clearly seen, and the bright- and dark-band contrasts are perfectly reversed. Because these banded contrasts are due to diffraction contrast, the bright bands in the (a) and (b) images correspond to the original A and B tetragonal variants, respectively. The striking feature of these images is that the striation contrast is missing in the B variant of the (b) image with $\mathbf{g}=002_B$. This absence suggests that the transition from the F_T phase with the $\langle 001\rangle$ polarizations results in the introduction of the [110] or $[1\bar{1}0]$ polarization component, which is perpendicular to $\mathbf{g}=002_B$. We thus checked the contrasts in the (c) and (d) images with $\mathbf{g}=110$ and $-\mathbf{g}=1\bar{1}0$ on the basis of the failure of Friedel's law. As suggested above, actually, the striation contrast is seen in the B variant. The striation contrast in these images exhibits two features: first, that one striation consists of a pair of fine, bright and dark stripes with an average width of about 20 nm, and second, that a gray region separates two neighboring pairs. Because the contrasts of the fine bright and dark stripes are reversed in these images, thus, the bright stripe is confirmed to have the [110] component for (c) and the $[1\bar{1}0]$ one for (d), both of which are parallel to the stripe direction. In addition, the polarization in the original tetragonal B variant should be parallel to the [001] direction.

Based on these results, we propose the following domain-structure model for domain I. The polarization direction determined for each domain in the area marked by the dotted square in (d) is shown in Fig. 4(e). As is indicated by the arrows, the bright and dark stripes, and the gray region, respectively, have their polarizations along the [110]+[001], $[1\bar{1}0]$+[001], and [001] directions. In other words, the F_T phase with the [001] polarization still exists in the gray region. Thus we identify domain I as a two-phase state consisting of the F_M and F_T phases. It was also found that a further cooling below room temperature was needed to obtain the single F_M phase, although the experimental data concerning this is not shown here.

To confirm that the striation contrast originates from the introduction of the $\langle 110\rangle$ components into the F_T phase, we have examined the crystallographic features of the reverse $F_M \rightarrow F_T$ transition by *in situ* observation using the transmission electron microscope. The dark field images in Figs. 5(a)–5(c) were, respectively, taken from the $x=0.47$ sample at 293, 371, and 478 K in the heating process from room temperature. The electron beam incidence in these images is parallel to the $[\bar{1}10]$ direction, and the 002 reflection for one original tetragonal variant was used to obtain these images. Both the banded and striation contrasts characterizing domain I in the F_M phase are clearly seen in (a) at 293 K. When the temperature is raised from 293 K, the striation contrast becomes faint and disappears around 430 K, which is the transition temperature of the reverse transition. Figure 5(c) at 478 K actually exhibits only the banded contrast due

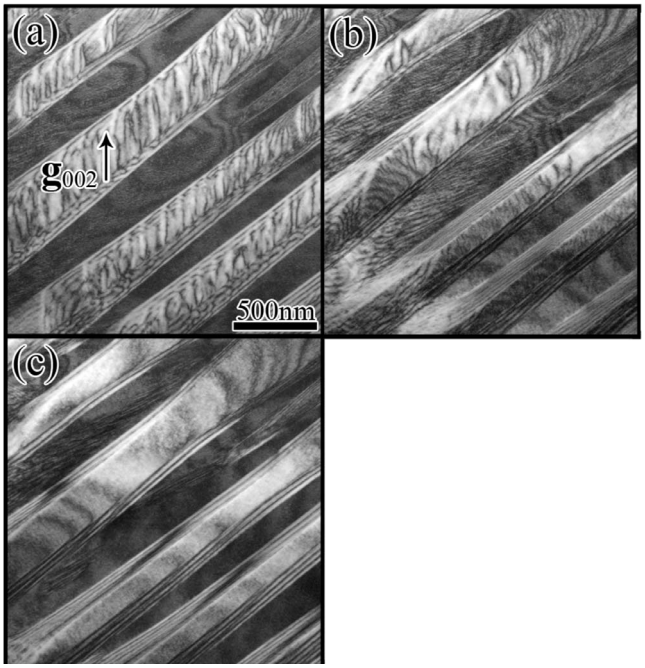

FIG. 5. Reverse phase transition from the F_M phase to the F_T phase on heating. The images were taken using the 002 reflection from the $x=0.47$ sample at (a) 293 K (room temperature), (b) 371 K, and (c) 478 K. Domain I at room temperature in the F_M phase is converted into the tetragonal banded domain structure around 370 K by an annihilation of striation-contrast regions.

to the 90° domain structure in the F_T phase. In other words, no change occurs in the banded contrast in the reverse transition. This fact is clearly direct evidence that the $F_T \rightarrow F_M$ transition on cooling is characterized only by the introduction of the $\langle 110\rangle$ polarization components, which gives rise to the striation contrast in the dark field images.

D. Crystallographic features of ferroelectric domain structures in F_R phase

The F_R domain structure at room temperature near the MPB was found to be a usual type of structure with straight domain boundaries, as is shown in the image (D) of Fig. 3. Before discussing the experimental data concerning domain II in the F_M-phase side of the MPB, we describe the results for both the domain-structure analysis of the F_R domain structures, including the usual room-temperature structure, and the change in domain structures with respect to temperature in the F_R side. Figure 6 shows four dark field images of the domain structure in the $x=0.42$ sample at room temperature. The images in (a)–(d) were taken using, respectively, the $\mathbf{g}=002$, $00\bar{2}$, 110, and $1\bar{1}0$ reflections. Note that the image in Fig. 6(a) is the same as that in image (D) in Fig. 3. Figures 6(a) and 6(b) clearly exhibit the F_R domain structure, detected as bright- and dark-contrast regions. The important feature in them is that the identity of the bright- and dark-contrast regions are reversed in the two images. This result provides evidence that the bright-contrast regions in Figs. 6(a) and 6(b) have polarization components parallel, respectively, to the [001] and $[00\bar{1}]$ directions. On the other hand,

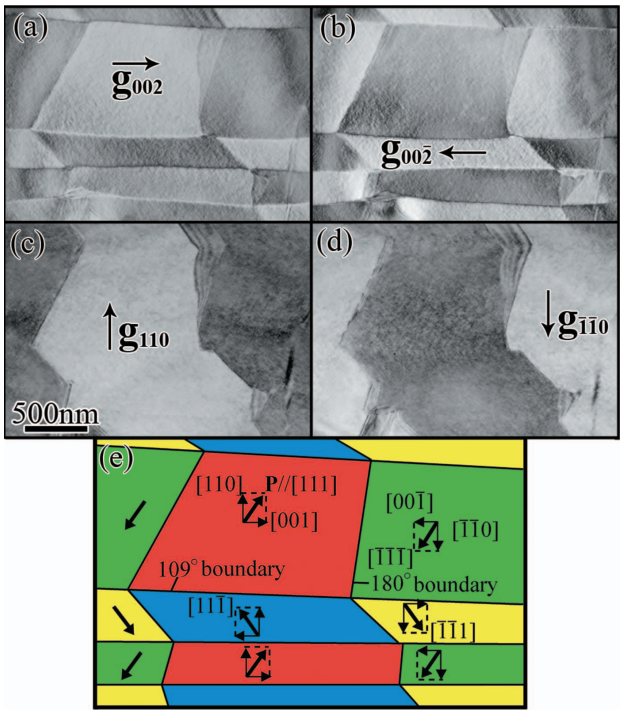

FIG. 6. (Color) Dark field images of the domain structure at room temperature in the F_R phase, together with the result of the domain-structure analysis. The images were taken from the same area of the $x=0.42$ sample at room temperature, with $g=$(a), 002, (b) 00$\bar{2}$, (c) 110, and (d) 1$\bar{1}$0 in the [$\bar{1}$10] electron beam incidence. In result (e), the solid arrow indicates the resultant polarization-vector direction in each domain, which is a sum of the ⟨001⟩ and ⟨110⟩ components.

the bright- and dark-contrast regions in Figures 6(c) and 6(d) are different from those in Figs. 6(a) and 6(b), but each is the reverse of the other. In this case, the [110] and [$\bar{1}$10] components are involved in the respective bright-contrast regions of Figs. 6(c) and 6(b). On the basis of these results, we determined the domain structure at room temperature, which is schematically depicted in Fig. 6(e). The schematic diagram shows that the determined F_R domain structure at room temperature consists of the usual 180° and 109° boundaries with the rhombohedral ⟨111⟩ polarization directions. In spite of these common features, we have to keep in our mind that many nanometer spotty areas are present in the interior of each domain, as seen in Figs. 6(a) and 6(b) with **g**=002 and 00$\bar{2}$.

To examine the detailed features of the changes in the [001]- and [110]-component areas as a function of temperature, the $x=0.42$ sample exhibiting the usual F_R domain structure was heated from room temperature to 660 K, a value above the T_C. Note that the temperature dependence of ε' in Fig. 2 indicates the T_C of 653 K. Figure 7 shows three pairs of dark field images of the same area, taken at 300, 620, and 660 K, using **g**=002 and 110. At 300 K, Fig. 7(a′) with **g**=002 exhibits the 109° and 180° domain boundaries, as was seen in Fig. 6(a), while only the 180° boundary is detected in Fig. 7(a) with **g**=110.

When the temperature is raised to 620 K, a value below T_C, the same [110]-component area still exists in Fig. 7(b)

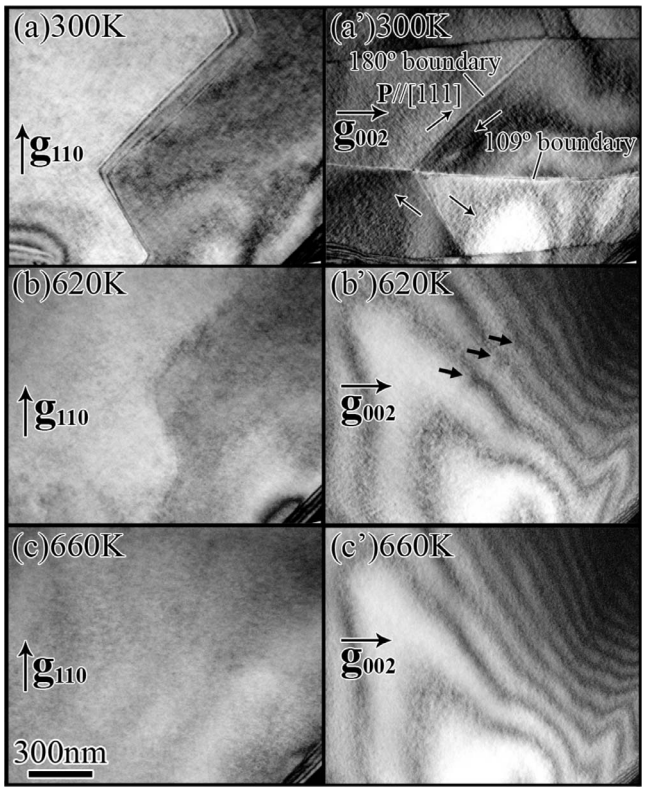

FIG. 7. Change in the [001]- and [110]-component areas in the heating process for the $x=0.42$ sample exhibiting the usual F_R domain structure at room temperature. The dark field images indicating the change in these component areas were taken at 300 K, (a) and (a′), 620 K, (b) and (b′), and 660 K, (c) and (c′), using the 110 and 002 reflections in the ($\bar{1}$10) electron incidence. The heavy arrows in the (b′) image indicate the anomaly in the contour regions, which is due to the presence of the boundary between the [110]- and [1$\bar{1}$0]-component areas.

with **g**=110, in spite of its relatively weak contrast. On the other hand, Fig. 7(b′) with **g**=002 clearly indicates that the domain structure consisting of the 109° and 180° boundaries is collapsed into a domain structure of nanometer-sized, spotty areas. It should be remarked that the boundary between the [110]- and [$\bar{1}$10]-component areas can be detected as an anomaly in the contour regions, as indicated by the thick arrows. As a result of the collapse of the [001]-component area, then, the ferroelectric domain structure between about 600 K and T_C can be identified as a nanometer-sized domain structure. When the temperature was further raised above T_C, the large [110]-component area was annihilated at T_C, and the sample transformed into the P_C phase, as seen in Fig. 7(c) at 660 K. In the F_R side of the MPB, it was thus found that there existed a continuous change, as a function of temperature, between the usual and the nanometer-sized domain structures.

The above-mentioned data revealed that the change between the usual and nanometer-sized domain structures occurred in the F_R side of the MPB. To clarify the crystallographic featrures of the change, and in particular, the collapse of the usual domain structure, we took a series of dark field images during the domain-structure change. The

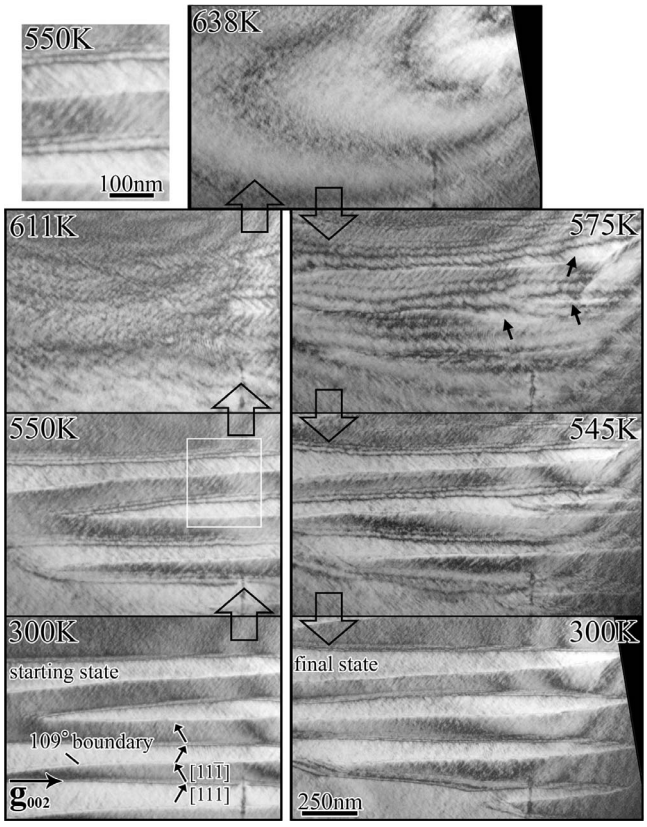

FIG. 8. Series of dark field images indicating the continuous and reversible change between the usual and nanometer-sized domain structures in the F_R side of the MPB. These images were taken from the same area of the $x=0.42$ sample, with $g=002$ in the $[\bar{1}10]$ electron incidence. To clearly show the arrangement of nanometer domains produced by a local conversion of the ⟨001⟩ components, we also provide the enlarged image of the region surrounded by the white lines in the image at 550 K in the top-left figure.

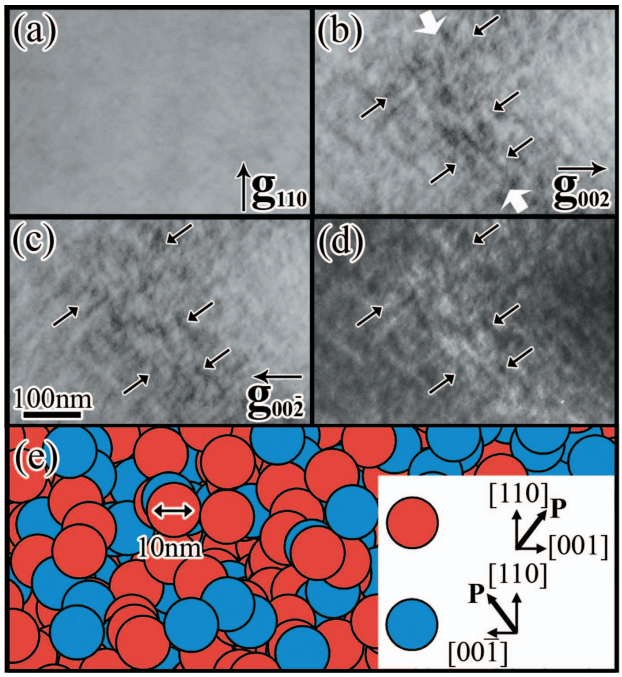

FIG. 9. (Color) Dark field images used in the analysis of the nanometer-sized domain structure, together with its domain-structure model. These images were taken from the nanometer-sized domain structure of the $x=0.42$ sample at 638 K, with $g=$(a) 110, (b) 002, and (c) $00\bar{2}$ in the $[\bar{1}10]$ electron incidence. The image in (d) shows the calculated reverse image contrast of the (b) image. Friedel's law fails only in the contour region indicated by the white thick arrows. In the domain model (e), two types of nanometer domains with the [110]+[001] and [110]+[00$\bar{1}$] polarization vectors are assumed to have a circular shape with a diameter of 10 nm.

images shown in Fig. 8 were obtained from the same area of the $x=0.42$ sample with $T_C=653$ K in the heating and subsequent cooling processes between 300 and 700 K. Note that our observation was carried out for a single [110]-component area to avoid the complexity resulting from the presence of many areas with different polarization components. The starting state at 300 K is characterized by the banded contrast, a result indicating the 109° domain structure seen in the left-bottom image. When the sample is heated from 300 K, the banded contrast becomes faint, and collapses around 600 K, as in the left-side images at 550 and 611 K. In order to understand the detailed change in the collapse, we carefully examined the enlarged image of the area surrounded by the white lines in the image at 550 K. In the enlarged image, there exist bright spotty areas aligned along the [111] direction in the dark $\mathbf{p}\|[11\bar{1}]$ domain, and dark spotty areas along the $[11\bar{1}]$ direction in the bright $\mathbf{p}\|[111]$ domain. Apparently, the usual domain structure is collapsed when the number of these spotty areas increases beyond a certain value. As a result of the collapse, many nanometer spotty areas are then distributed uniformly in the nanometer-sized domain structure, as seen in the image at 638 K.

To further examine the domain-structure change in the cooling process, the same sample was cooled down from 638 K to room temperature, as is shown in the right-side images of Fig. 8. When the temperature is lowered from 638 K, the nanometer spotty areas in the nanometer-sized domain structure tend to align along the [111] or $[11\bar{1}]$ direction in the image at 575 K. A notable feature in this image is that larger, bright-contrast areas appear locally, generated by a coalesence of spotty areas, as marked by the arrows in the image. On the basis of the images at 545 and 300 K, we find that after these larger, bright-contrast areas develop, the usual 109° domain structure forms. That is, the change between the nanometer-sized and usual domain structures is continuous and reversible. Because the usual F_R domain structure is formed by a coalesence of nanometer spotty areas, each domain in it can be regarded as an aggregation of nanometer ferroelectric domains.

We here describe the result of the analysis of the nanometer-sized domain structure appearing just below the T_C of 653 K. Figure 9 shows three dark field images of a single [110]-component area in the $x=0.42$ sample at 638 K. The images in Figs. 9(a)–9(c) were taken with $\mathbf{g}=110$, 002, and $00\bar{2}$, and the calculated image in Fig. 9(d) was obtained by a contrast reversal of Fig. 9(b). Looking first at the image with $\mathbf{g}=110$, we detect no notable contrast in it because of the single [110]-component area. On the other hand, spotty-contrast areas, estimated to be about 10 nm in average size,

appear in the images with $\mathbf{g}=002$ and $00\bar{2}$. In order to check the positional relationship between the bright and dark spotty areas, we compared the contrasts between the experimental (c) and calculated (d) images, selecting the contour region indicated by the thick arrows. We did so because Friedel' law fails only in a region where the Bragg condition is satisfied under the two-beam condition. As the thin arrows indicate, the bright and dark spotty areas present along the contour region are basically identical to each other in size and shape. The polarization components of the bright areas in Figs. 9(b) and 9(c) are then parallel to the [001] and $[00\bar{1}]$ directions, respectively. A model of the nanometer-sized domain structure determined on the basis of these features is depicted in Fig. 9(e). In the model, two types of domains with [110] +[001] and $[110]+[00\bar{1}]$ polarization vectors are uniformly distributed in space. Because the ratio between the magnitudes of the [110] and ⟨001⟩ components is not restricted to $\sqrt{2}:1$, the direction of the polarization vector in each nanometer domain does not need to be parallel to one of the rhombohedral ⟨111⟩ directions. In this study, however, we could not determine whether a crystal symmetry of a nanometer domain is rhombohedral or monoclinic.

As was mentioned just above, two types of nanometer domains in the nanometer-sized domain structure have the $[110]+[001]$ and $[110]+[00\bar{1}]$ polarization vectors. Thus the appearance of nanometer domains before the collapse in the heating process, as in the image at 550 K of Fig. 8, must be directly associated with a local conversion between the [001] and $[00\bar{1}]$ polarization components. That is, when the [001] component in a rhombohedral [111] domain is, for instance, converted locally into the $[00\bar{1}]$ component, a nanometer domain with the $[110]+[00\bar{1}]$ vector appears in the original [111] domain. In addition to these features, we should note the following fact: an average ⟨001⟩ component must be zero in a large [110]-component area. With the spatial cancellation of the ⟨001⟩ components, the nanometer-sized domain structure consisting of nanometer ferroelectric domains can be regarded as an aggregation-type domain structure with average orthorhombic symmetry. Note that each large [110]-component area should correspond to one orthorhombic domain in the aggregation-type domain structure.

E. Crystallograpic features of domain II appearing in the F_M phase near the MPB

The usual room-temperature domain structure in the F_R side of the MPB was understood to be an aggregation-type with rhombohedral symmetry. With this result in mind, we examined the characteristic features of the domain II appearing in the F_M side of the MPB by taking dark field images with various **g** vectors. For this domain, we wished to clarify the identity of a nanometer spotty area observed within it. Five dark field images of the same area in the interior of one of the domains are shown in Fig. 10. The images in Figs. 10(a)–10(e), respectively, were taken from the $x=0.46$ sample at room temperature, with $\mathbf{g}=002$, $\bar{1}\bar{1}1$, 112, 121, and 111. The $(\bar{1}10)$ pole figure indicating the directions of these **g** vectors is also provided. Of these images, the 002 image

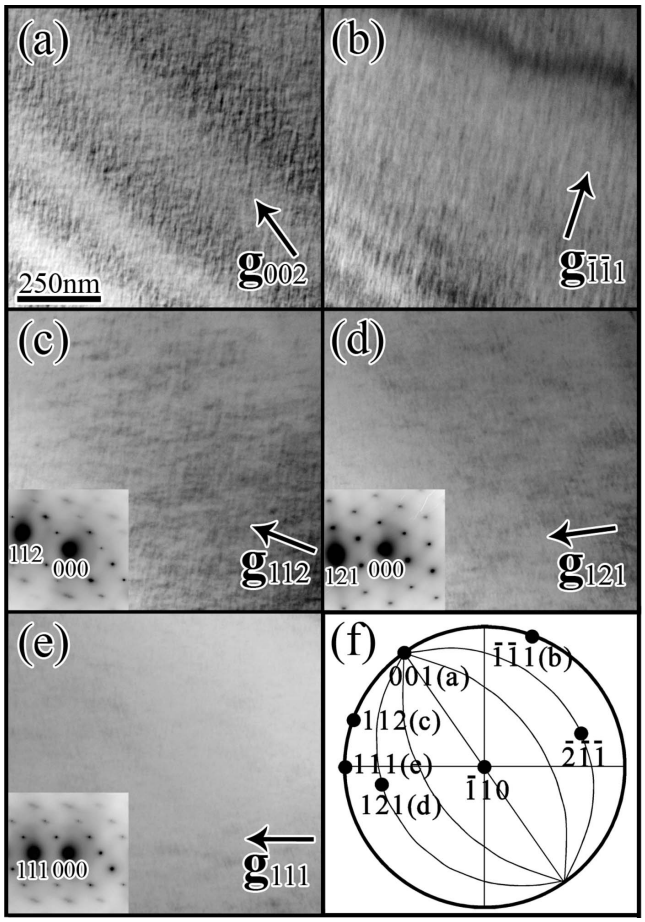

FIG. 10. G-vector dependence of contrast in the dark field images for domain II in the F_M phase, together with the $(\bar{1}10)$ pole figure. The images were taken from the $x=0.46$ sample at room temperature, using the (a) 002, (b) $\bar{1}\bar{1}1$, (c) 112, and (e) 111 reflections in the $[\bar{1}10]$ electron incidence, while the 121 reflection in the $[\bar{1}1\bar{1}]$ incidence was used for the image in (d). The electron diffraction patterns corresponding to the images in (c), (d), and (e) are also shown in the insets. In (f), the $(\bar{1}10)$ pole figure shows the orientation relationship between (a), (b), (c), (d), and (e).

exhibits the bright-contrast spotty areas, as is seen in the $x=0.46$ image in Fig. 3(c). In order to understand the origin of these areas, we turned to the image in which $\mathbf{g}=\bar{1}\bar{1}1$. The fine striation contrast, usually called a tweed pattern, along the $[\bar{1}\bar{1}1]$ direction appears in the $\bar{1}\bar{1}1$ image. According to several studies on ferroelastic phase transitions, a strain field produced by the presence of nanometer regions generates this tweed pattern.[18–21] Thus these areas should reflect nanometer ferroelectric regions arranged along the $[\bar{1}\bar{1}1]$ direction; such regions may be F_M domains with polarization vectors P_M nearly parallel to the ⟨112⟩ directions.[22]

We then focused on the images in which $\mathbf{g}=112$ and 121, together with the corresponding $[\bar{1}10]$ and $[\bar{1}1\bar{1}]$ electron diffraction patterns in the insets. Note that, because the [112] direction is normal to [111], the contrast due to the strain field is completely missing in the [112] image. That is, we can get only contrast due to ferroelectric domains themselves. In these images and patterns, the striking features are

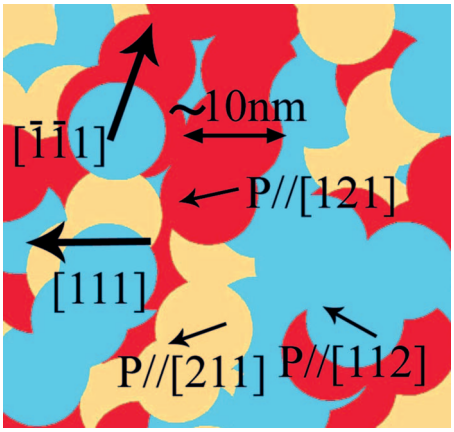

FIG. 11. (Color) Proposed domain-structure model of domain II in the F_M phase near the MPB. In the model, the size and shape of the nanometer F_M domains are assumed to be about 10 nm and circular on the basis of the bright-contrast areas in the 002 image of Fig. 10(a).

that, surprisingly, the intensities of the 112 and 121 reflections in the patterns are slightly stronger than that of the direct 000 reflection, and that, correspondingly, the 112 and 121 images produce the brightest contrast in the whole area, a situation allowing the detection of dark-contrast spotty areas. These observations indicate that, as an individual domain cannot be separately detected, nanometer domains with polarizations nearly parallel to the [112] and [121] directions are uniformly distributed throughout this whole area. In addition, there is no notable contrast in the image in which $\mathbf{g}=111$ near $\mathbf{g}=112$ and 121. This absence is indicative of the fact that, because the polarization vectors $\mathbf{P_M}\|[112]$, [121], and [211] have the same value of $\mathbf{g}\cdot\mathbf{P_M}$ for $\mathbf{g}=111$, nanometer domains with the [211] polarization should also be present in this area. It should further be remarked that images with $\mathbf{g}=110$, not shown here, were found to exhibit a nanometer spotty contrast. In other words, there is no large polarization-component areas in domain II, unlike the [110]-component area in the nanometer-sized domain structure of the F_R side.

Based on the above experimental data, we propose the model of domain II shown in Fig. 11. In the model, each domain in domain II is an aggregation of three types of nanometer monoclinic domains, which tend to align along the [$\bar{1}\bar{1}$1] direction. The polarization vectors of the three nanometer domains are nearly parallel to the [112], [121], and [211] directions around the [111] direction. Note that the [111] direction is obviously one of the polarization directions of the F_R phase. Because the intensities differ among the 112, 121, and 211 reflections in the diffraction patterns, the number of these types of nanometer domains should not be equal to one another. This inequality results in the deviation of the average polarization direction from the rhombohedral [111] direction. It is thus understood that, as a total, each of the domains in domain II have a certain polarization direction, presumably a triclinic direction.

According to the literature-reported phase diagram in Fig. 1, the $x=0.46$ sample should undergo the phase transition to

FIG. 12. Series of dark field images indicating the domain-structure change in the F_M side of the MPB. These images were taken at (a) 293 K before heating, and at (b) 603 K, (c) 490 K, and (d) 293 K on subsequent cooling, using the 102 reflection in the [21$\bar{1}$] electron incidence. When the temperature was raised above about 490 K, the new banded domain structure appeared in the interior of each domain in domain II.

the F_T phase on heating, just as in the case of the $x=0.47$ sample. However, the monoclinic domain structure, domain II, in $x=0.46$ is quite different from that of domain I in $x=0.47$. In order to understand the origin of the difference, we conducted *in situ* observations of the phase transition between the F_M and F_T phases. Figure 12 shows four dark field images of the same area in the $x=0.46$ sample in the heating and subsequent cooling processes between room temperature and 603 K. These images were actually taken at (a) 293 K before heating, at (b) 603 K, (c) 490 K, and (d) 293 K on cooling, using the 102 reflection in the [21$\bar{1}$] electron beam incidence. The reason for the adoption of the [21$\bar{1}$] incidence, instead of the [110] incidence in Fig. 10, is that the

overall features of a domain-structure change in the $x=0.46$ sample could easily be detected in this incidence. In other words, the contrast that the nanometer domains create, which is clearly present in the [110] incidence, is not apparent in the $[21\bar{1}]$ incidence.

In Fig. 12(a), taken at 293 K before heating, domain II with curved boundaries is observed as the initial state. When we heated the sample from 293 K, we could detect the appearance of a new banded domain structure with a width of about 20 nm, as seen in Fig. 12(b). The characteristic features of this new structure are that a domain boundary is not parallel to a crystallographic plane with a lower index, and that the original domain boundaries in domain II still exist, though they are slightly changed. When the temperature was then lowered from 603 K, the new banded structure was annihilated at a T_T of about 490 K, as seen in Figs. 12(c) and 12(d). Interestingly, the temperature T_T is almost identical to the transition temperature of the teteragonal-to-monoclinic transition in the phase diagram of Fig. 1. The reversible change in the domain structures at T_T obviously indicates the presence of a new phase transition between two ferroelectric phases. In other words, the appearance of the banded structure on heating reflects a lowering of crystal symmetry. Thus the new transition appears not to be the transition between the F_M and F_T phases. In addition, some of the bands in the banded structure were not sometimes annihilated in the cooling process. At a later point, we will discuss the details of the phase transition in the F_M side, including the survival of some of the bands.

Finally, in order to understand the correlation between the domain structure and the large piezoelectric response near the MPB, we examined the characteristic features of a domain structure at room temperature in poled samples with $x=0.46$. To obtain the poled samples, we heated the $x=0.46$ sample from room temperature to about 450 K and then cooled it down under an electric field of about 30 kV/cm. Figure 13 shows two dark field images indicating a domain structure in a poled sample. These images were taken from the same area at room temperature, using the 102 reflection in the $[21\bar{1}]$ incidence direction, but Fig. 13(b) was obtained by a very slight rotation of the sample from the incidence direction for Fig. 13(a). The reason for the rotation was that, owing to severe sample distortion, the Bragg condition was difficult to fulfill in a wider area. On the basis of both images, we found that the banded domain structure had formed in the interior of almost every domain of domain II. This banded structure is very similar to that obtained by the sample heating above T_T. In particular, the domain boundary is not parallel to one of the crystallographic planes with low indexes. Evidently, then, an application of an electric field to a sample exhibiting domain II is equivalent to heating the sample. The appearance of the high-temperature phase in the F_M side of the MPB is likely to play an essential role in the large piezoelectric response in PZT.

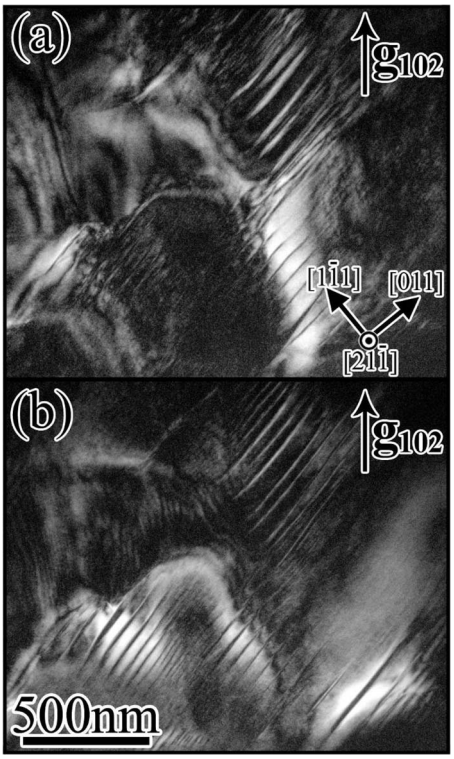

FIG. 13. Two dark field images of domain structure in a poled sample with $x=0.46$. Both images were taken from the same area at room temperature, using the 102 reflection, basically in the $[21\bar{1}]$ electron incidence. However, the incidence in (b) is slightly rotated from that in (c), owing to severe distortion of the sample. In the images, the banded domain structure is clearly observed in the interior of each domain in domain II with curved boundaries.

IV. DISCUSSION

The experimental data in this study revealed that at room temperature near the MPB there existed two types of ferroelectric domain structures, referred to as domains I and II in the F_M phase, in addition to the usual structure consisting of 109° and 180° boundaries in the F_R phase. Of the two monoclinic domain structures, domain I in $0.47 \leqslant x \leqslant 0.50$ was produced as a result of the $F_T \rightarrow F_M$ phase transition accompanying the introduction of the $\langle 110 \rangle$ polarization components. In contrast, domain II in $x=0.46$ near the MPB is characterized by curved domain boundaries, and each domain in it is identified as an aggregation of three types of nanometer ferroelectric domains. The interesting feature is that, in the usual room-temperature structure in the F_R side of the MPB, each domain also appears to be an aggregation of two types of nanometer domains. In other words, the room-temperature domain structures in both sides of the MPB can be referred to as an aggregation-type domain structure.

Our *in situ* observations showed that, when the temperature was lowered from the P_C phase, a coalescence of nanometer domains in the nanometer-sized domain structure, formed just below the T_C, produced the usual F_R domain structure. Although the crystal symmetry of a nanometer domain is monoclinic or rhombohedral, the nanometer-sized domain structure was also suggested to be an aggregation-type with average orthorhombic symmetry. In the F_M side of the MPB, on the other hand, heating from room temperature resulted in the formation of the new banded domain structure at T_T. Because the banded domain structure was basically

annihilated at T_T on subsequent cooling, the new phase transition most likely occurs in the F_M side. In addition, we noted a similar banded domain structure in the interior of each domain of domain II in poled samples with $x=0.46$. Because an excellent piezoelectric response was obtained near the MPB in the poled samples, the new phase transition producing the banded domain structure is likely to be crucial for an understanding of the excellent response in PZT.

A continuous and reversible change between the usual and nanometer-sized domain structures existed in the F_R side of the MPB. In our opinion, the nanometer-sized domain structure is an aggregation-type domain structure with average orthorhombic symmetry; our reasoning is that an average $\langle 001 \rangle$ polarization component must be zero in a large [110]-component area coresponding to an orthorhombic domain. Based on this feature, the origin of the domain-structure change in the F_R side is connected with the result that the collapse of the usual domain structure on heating is directly associated with a local conversion between the [001] and $[00\bar{1}]$ polarization components. In fact, it seems that the collapse originates in the increase in the number of nanometer domains, which are produced by a local conversion, beyond a certain value. Although we could not determine whether a symmetry of a nanometer domain in the nanometer-sized doamin structure is monoclinic or rhombohedral, it seems to us that the occurance of a local conversion is associated with the rhombohedral-to-monoclinic symmetry change in a nanometer domain. If so, this symmetry change must be responsible for the collapse of the usual domain structure. In the senario based on the symmetry change in a nanometer domain, further, the formation of the usual domain structure from the nanometer-sized structure can be explained in the following way. That is, the nanometer domains in the nanometer-sized domain structure are first rearranged along the $\langle 111 \rangle$ directions; when they coalesce, larger areas, indicated by the arrows in Fig. 8, appear. The usual domain structure was then formed by the growth of these larger areas. Based on this senario, thus, a monoclinic-to-rhombohedral symmetry change in the cooling process may occur in a nanometer domain with the appearance of such areas.

Domain II, as an aggregation-type domain structure, was found to be present in the F_M side of the MPB. When the $x=0.46$ sample exhibiting domain II was heated from room temperature, the new, banded domain structure was formed in the interior of each domain of domain II at T_T, which corresponds to the transiton temperature between the F_T and F_M phases in the phase diagram of Fig. 1. This domain structure is basically annihilated at T_T on subsequent cooling, a result which indicates that the phase transition exists. However, the appearance of the banded structure suggests that the transition is different from that between the F_M and F_T phases.

In order to understand the features of the new phase transition, we focus on two points: first, that the appearance of the banded domain structure on heating reflects a lowering of the crystal symmetry, and second, that the banded structure is one of the aggregation-type domain structures. It is obvious that a crystal symmetry lower than monoclinic can only be triclinic. In that case, the higher- and lower-temperature phases in the F_M side of the MPB possess triclinic and monoclinic symmetries, respectively. Furthermore, because the domain structures in these phases are of an aggregation type, the symmetry change may occur in a nanometer domain. Thus the reversible change in the banded domain structure should be attributed to the phase transition between the triclinic and F_M phases, which is associated with the symmetry change in a nanometer domain. In this scenario also, the polarization vector for each nanometer domain in the triclinic phase does not necessarily return to an original monoclinic vector in the symmetry change on cooling. In the F_R side, in fact, such a large vector change, produced by a local $\langle 001 \rangle$ conversion, actually occurs in the domain-structure change. This polarization vector irreversiblity in the transition could thus account for the survival of some bands in the cooling process.

The excellent piezoelectric response was obtained in poled samples having the Zr content near the MPB.[1–4] In this study, we subjected samples exhibiting domain II to the poling process. In the dark field images of Fig. 12, the banded domain structure with an average width of about 20 nm exists in the interior of each domain of domain II. An interesting feature of the banded structure is that the domain boundary is not parallel to one of the crystallographic planes with lower indexes. Hence this feature is entirely consistent with that of the banded structure obtained by the sample heating above T_T. This implies that the application of an electric field induces the phase transition to the triclinic phase. Based on this result, it is suggested that the triclinic phase should play a crucial role in the appearance of the excellent piezoelectric response in PZT.

Finally, we turn to the origin of the appearance of the aggregation-type domain structures near the MPB in PZT. In this paper, the aggregation-type domain structure is defined as a ferroelectric domain structure, each domain of which comprises an aggregation of nanometer domains with an average size of about 10 nm. The important feature for the understanding of the origin of this appearance is that the crystal symmetries of the nanometer domains found in this strudy are triclinic for the banded domain structure, monoclinic for domain II, monoclinic or rhombohedral for the nanometer-sized domain structure, and rhombohedral for the usual room-temperature F_R domain structure. Because nanometer domains are formed at the T_C, in particular, it seems that the triclinic and monoclinic symmetries are crucial for their appearance. That is, the weak crystallographic constraint resulting from such reduced symmetries should allow remarkable local fluctuations of a polarization vector. In addition, due to the *B*-site disordering in the PZT, local fluctuations would be enhanced by a random electric field. These fluctuations then bring about the formation of a nanometer domain. This hypothesis leads us to conclude that these two factors, a lower symmetry and a random field, must be responsible for the appearance of the aggregation-type domain structures.

V. CONCLUSIONS

The present room-temperature and *in situ* transmission electron microscope observations reveal that four types of

aggregation-type ferroelectric domain structures exist near the MPB in PZT. The striking feature of these structures is that each domain is an aggregation of nanometer domains with an average size of about 10 nm. Among them, the domain II and the banded domain structure in the F_M side of the MPB can, respectively, be identified as aggregation-type structures in the low-temperature F_M and high-temperature triclinic phases. In the F_R side, the usual F_R domain structure consisting of the 109° and 180° boundaries at room temperature are also of an aggregation type, and its nanometer domain has rhombohedral symmetry. When the temperature is raised from room temperaure, the usual domain structure is converted into the nanometer-sized domain structure consisting of nanometer ferroelectric domains. Because an average $\langle 001 \rangle$ polarization component must be zero in a large [110]-component area, the nanometer-sized domain structure can be regarded as an aggregation-type structure with average orthorhombic symmetry. In addition, the application of an electric field to samples exhibiting domain II resulted in the appearance of the banded domain structure, the same as that which was obtained by heating the sample. This result indicates that the presence of the triclinic phase is crucial for the appearance of the excellent piezoelectric response in PZT.

ACKNOWLEDGMENTS

This work was partially supported by the Murata Science Foundation and by a Waseda University Grant for Special Research Projects (2005B-271, 2005B-150).

[1] M. E. Lines and A. M. Glass, *Principles and Applications of Ferroelectrics and Related Materials* (Clarendon, Oxford, 1979).
[2] K. Uchino, *Piezoelectric Actuators and Ultrasonic Motors* (Kluwer Academic, Boston, 1996).
[3] A. Antonio, *Piezoelectric Transducers and Applications* (Springer, Berlin, 2004).
[4] B. Jaffe, W. R. Cook, and H. Jaffe, *Piezoelectric Ceramics* (Academic Press, London, 1971).
[5] W. Cao and L. E. Cross, Phys. Rev. B **47**, 4825 (1993).
[6] S. K. Mishra, D. Pandey, and A. Singh, Appl. Phys. Lett. **69**, 1707 (1996).
[7] X-h. Du, J. Zheng, U. Belegundu, and K. Uchino, Appl. Phys. Lett. **72**, 2421 (1998).
[8] M. Hammer, C. Montry, A. Endriss, and Michel J. Hoffmann, J. Am. Ceram. Soc. **81**, 721 (1998).
[9] B. Noheda, D. E. Cox, G. Shirane, J. A. Gonzalo, L. E. Cross, and S-E. Park, Appl. Phys. Lett. **74**, 2059 (1999).
[10] R. Guo, L. E. Cross, S-E. Park, B. Noheda, D. E. Cox, and G. Shirane, Phys. Rev. Lett. **84**, 5423 (2000).
[11] B. Noheda, J. A. Gonzalo, L. E. Cross, R. Guo, S-E. Park, D. E. Cox, and G. Shirane, Phys. Rev. B **61**, 8687 (2000).
[12] B. Noheda, D. E. Cox, G. Shirane, R. Guo, B. Jones, and L. E. Cross, Phys. Rev. B **63**, 014103 (2000).
[13] Z.-G. Ye, B. Noheda, M. Dong, D. Cox, and G. Shirane, Phys. Rev. B **64**, 184114 (2001).
[14] L. Bellaiche, A. García, and D. Vanderbilt, Phys. Rev. B **64**, 060103(R) (2001).
[15] M. Tanaka and G. Honjo, J. Phys. Soc. Jpn. **19**, 951 (1964).
[16] F. J. Fujimoto, J. Phys. Soc. Jpn. **14**, 1558 (1959).
[17] T. Asada and Y. Koyama, Phys. Rev. B **70**, 104105 (2004).
[18] A. G. Khachaturyan, *Theory of Structural Transformations in Solids* (Wiley, New York, 1983).
[19] T. Onozuka, N. Ohnishi, and M. Hirabayashi, Metall. Trans. A **19**, 797 (1998).
[20] L. E. Tanner, A. R. Pelton, and R. Gronsky, J. Phys. (France) **43**, C4–169 (1982).
[21] S. Muto, S. Oshima, and F. E. Fujita, Acta Metall. Mater. **38**, 685 (1990).
[22] J. M. Kiat, Y. Uesu, B. Dkhil, M. Matsuda, C. Malibert, and G. Calvarin, Phys. Rev. B **65**, 064106 (2002).